Experimental model inverse-based hysteresis compensation on a piezoelectric actuator

Raouia Oubellil
Univ. Grenoble Alpes,
GIPSA-Lab,
F-38000 Grenoble, France
CNRS, GIPSA-Lab,
F-38000 Grenoble, France
raouia.oubellil@gipsa-lab.grenoble-inp.fr,

Łukasz Ryba and Alina Voda
Univ. Grenoble Alpes, GIPSA-Lab,
F-38000 Grenoble, France
CNRS, GIPSA-Lab,
F-38000 Grenoble, France
lukasz.ryba@gipsa-lab.grenoble-inp.fr,
alina.voda @gipsa-lab.grenoble-inp.fr

Micky Rakotondrabe
FEMTO-ST Institute,
AS2M department,
Univ. Bourgogne Franche-Comté,
Univ. de Franche-Comté/CNRS/
ENSMM/UTBM, Besançon, France,
mrakoton@femto-st.fr

***Abstract*—This paper presents a comparison of several open-loop methods for hysteresis compensation on a lab-made micro-/nanopositioning device. The classical Preisach model with the inverse multiplicative structure, and the Classical/Modified Prandtl-Ishlinskii models with model inversion, are considered. The classical Preisach method though suited for asymmetric hysteresis, does not have an analytic inverse model. However, it can be used directly in the inverse multiplicative structure, thus avoiding the computationally intensive numerical inversion of the Preisach model. The classical Prandtl-Ishlinskii (PI) model is accurate and has an analytic solution, which makes it interesting for real-time applications. However, the model captures only the symmetrical hysteresis curves. Modified Prandtl-Ishlinskii (MPI) model has all of the advantages of the classical PI model and extends it for asymmetric hysteresis. The considered methods are compared experimentally, and illustrative results are given for tracking triangular references of different frequencies.**

***Index Terms*—Piezoelectric actuator, micro/nanopositioning, hysteresis, Preisach model, Prandtl-Ishlinskii model, Modified Prandtl-Ishlinskii model.**

I. INTRODUCTION

Piezoelectric actuators (PEA's) are widely used at micro-/nanoscale (e.g. Scanning Tunneling Microscope (STM) [1] and Atomic Force Microscope (AFM) [2]) because of their simple configuration, high precision, fast response, and theoretically unlimited displacement. However, nonlinearities such as hysteresis, friction and creep, degrade system performance [3], especially hysteresis which remains a major limitation to the precision and causes positioning errors.

Various methods have been developed for hysteresis compensation and they can be generally divided into two categories: closed-loop and open-loop methods. The closed-loop techniques such as high gain feedback [4], H_∞ based control [5], disturbance observer [6], [7] have demonstrated a significant improvement of the control performance, but are limited w.r.t vibration dynamics compensation and are sensitive to measurement noise due to feedback-loop sensors. The open-loop techniques are mainly based on cascading the calculated inverse model of hysteresis with the real system leading to its linearization. The most common techniques include the Preisach model [8], [9], the Prandtl-Ishlinskii (PI) model [10], [11], [12], its modified version (MPI model [13]) for asymmetric hysteresis and the Bouc-Wen model [14]. Their performance is determined by the accuracy of the inverse model [15].

The hysteresis compensator can be constructed either by inverting the hysteresis model or by using this model directly in the inverse multiplicative structure [16], [17]. The classical Presiach model is accurate and suited for asymmetric hysteresis [18]. However, its inverse model cannot be found analytically, and the numerical solution can be computationally consuming or too complex to implement in real-time. To overcome this limitation, one possible solution is to use the hysteresis model in the inverse multiplicative structure [19]. Prandtl-Ishlinskii (PI) model is accurate, since it is derived from the Preisach model. Moreover, its inverse is analytic which makes it well suited for real-time applications [20]. However, classical PI model cannot capture asymmetric hysteresis loops. To that end, Modified Prandtl-Ishlinskii (MPI) model has been developed (see for example [21]).

In the literature, several alternative models to Preisach model have been proposed, which are computationally less cumbersome while having the same application range [22]. However, to the authors best knowledge, there is still a clear lack of studies that compare the open-loop compensation methods, of the Preisach and the alternative models, which could be really useful for practitioners. Therefore, in this paper, inverse classical and Modified Prandtl-Ishlinskii models are compared to the inverse multiplicative structure of the Preisach model, for hysteresis compensation of piezoelectric actuator in the horizontal axis of a lab-made micro-/nanopositioning device. The paper is organized as follows: the experimental setup is given in Section II. In section III the Preisach model and its inverse multiplicative compensator are presented. Section IV describes the classical and the Modified Prandtl-Ishlinskii models with the model inversion. The compensators are implemented in real-time and the experimental results are shown in Section V. Section VI concludes the paper.

II. EXPERIMENTAL SETUP AND SYSTEM DESCRIPTION

The experimental setup is a 3DOF micro-/nanopositioning

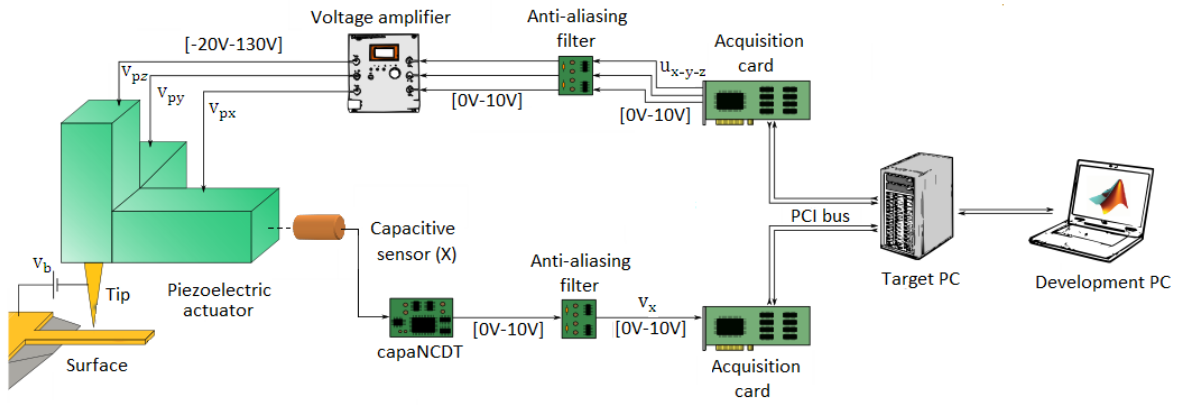

Fig. 1. Experimental setup of micro-/nanopositioning platform

platform developed at GIPSA-lab, Grenoble, France, shown in Fig. 1 (see also [7], [23]). However, in the present paper, only the horizontal (X) axis is considered. This axis is actuated with a piezoelectric actuator Tritor T-402-00 of gain 235 [nm/V] and bandwidth 630 Hz. A capacitive sensor CS005 (gain 200 [V/mm] and bandwidth 8.5 kHz) is used to measure the axis displacement. The applications are designed in Matlab&Simulink™ and xPC Target™ software on a development PC. The signal acquisition is performed with a sampling frequency of 20 kHz, using a Target PC equipped with data acquisition cards. The considered X axis ($Plant_x$) can be modeled as a cascade interconnection of a voltage amplifier $VA_x(s)$, the piezoelectric actuator $Piezo_x$ (hysteresis nonlinearity H_x, followed by linear piezo dynamics $D_p x(s)$) and the capacitive sensor $CS_x(s)$ as illustrated in Fig. 2. Since the bandwidth of the voltage amplifier and the bandwidth of the capacitive sensor are relatively high w.r.t. the bandwidth of the piezoactuator, they can be assumed as static gains (G_{vx} and G_{capx}, respectively). For static hysteresis identification, the frequency of the input signal is chosen relatively low (1 Hz) w.r.t the bandwidth of the piezoactuator (630 Hz), so that the piezo dynamics $D_{px}(s)$ can be neglected (i.e. $q_{px}(t) = x_p(t)$ in Fig. 2).

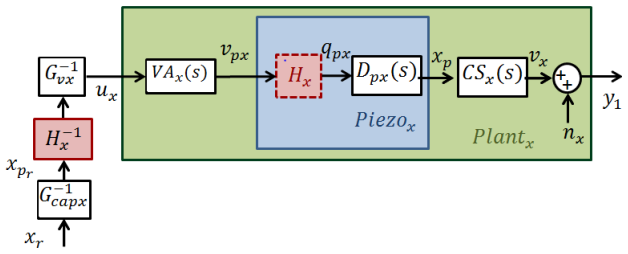

Fig. 2. Block diagram of the considered X axis with inverse-based hysteresis compensator.

III. Inverse Multiplicative Structure for Preisach Model

A. Classical Preisach model

Mathematically, the classical Preisach model can be written as [18]:

$$x_p(t) = H(v_{px}(t)) = \iint_{\alpha \geq \beta} \mu(\alpha, \beta)\gamma[v_{px}(t)]\, \mathrm{d}\alpha \mathrm{d}\beta \qquad (1)$$

where $\mu(\alpha, \beta)$ is the Preisach weighting function, $\gamma[v_{px}(t)]$ is the Preisach operator having an output of +1 or 0 and α, β are the upper and lower switching values of the input $v_{px}(t)$, respectively.

Assuming that $v_{px_{min}} \leq \beta \leq \alpha \leq v_{px_{max}}$, the operator $\gamma[v_{px}]$ can be represented by a simple 2-state relay with hysteresis (see Fig. 3(a)), and can be integrated over the limiting triangle T_0 as illustrated in Fig. 3(b).

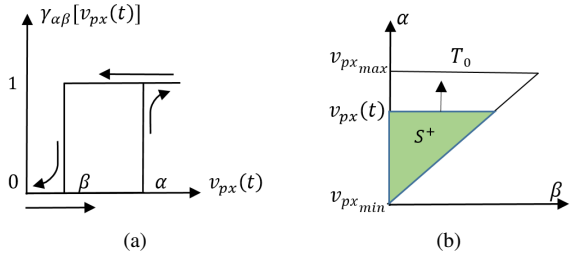

Fig. 3. Preisach model of hysteresis: (a) Elementary Preisach operator, (b) Integration over the limiting triangle T_0.

To define the final hysteresis operator, the elementary Preisach operators are multiplied by the weighting function $\mu(\alpha, \beta)$ and superposed as shown in (Fig. 4)

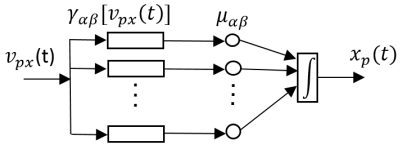

Fig. 4. Block diagram of the Preisach model.

So as to both simplify the calculation and suppress the double integration (1), the Preisach function is defined as follows:

$$X_p(\alpha, \beta) = x_{p_\alpha} - x_{p_{\alpha\beta}} \tag{2}$$

where x_{p_α} is the hysteretic system output once the input $v_{px}(t)$ is increased from 0 to α and $x_{p_{\alpha\beta}}$ is the system output once the input $v_{px}(t)$ is decreased from α to β.

If the hysteresis loop contains several extrema α_k, β_k, the total hysteretic output $x_p(t)$ for an input voltage $v_{px}(t)$ is determined by (2) depending on the current slope of $v_{px}(t)$ as follows:

$$\begin{aligned} &\dot{v}_{px}(t) > 0 \\ &x_p(t) = \textstyle\sum_{k=1}^{N} [X_p(\alpha_k, \beta_{k-1}) - X_p(\alpha_k, \beta_k)] \\ &\quad + X_p(v_{px}(t), \beta_N) \end{aligned} \tag{3}$$

$$\begin{aligned} &\dot{v}_{px}(t) < 0 \\ &x_p(t) = \textstyle\sum_{k=1}^{N-1} [X_p(\alpha_k, \beta_{k-1}) - X_p(\alpha_k, \beta_k)] \\ &\quad + X_p(\alpha_N, \beta_{N-1}) - X_p(\alpha_N, v_{px}(t)) \end{aligned} \tag{4}$$

The Preisach model still requires a property so called the *wipe-out property*, which allows to erase the pair (α_N, β_{N-1}) from the history once $v_{px}(t)$ exceeds α_N, and the pair (α_N, β_N) once $v_{px}(t)$ becomes smaller than β_N (see [24]).

For practical application in hysteresis compensation, equations (3) and (4) are based on an approximation of X_p as a polynomial expansion in α and β as follows:

$$\begin{aligned} X_p(\alpha, \beta) = \theta_0\beta + \theta_1\alpha + \theta_2\beta^2 + \theta_3\beta\alpha + \theta_4\alpha^2 \\ + \theta_5\beta^3 + \theta_6\beta^2\alpha + \theta_7\beta\alpha^2 + \theta_8\alpha^3 \end{aligned} \tag{5}$$

To identify the parameters θ: (i) A sinusoidal inputs of frequency 1 Hz and amplitudes from 0 to 120 V with a step of 5 V are applied. (ii) Values of $X_p(\alpha, \beta)$ for different pairs (α, β) are determined from these experimental hysteresis curves (see equation (2)). (ii) The Least Squares method is used and the following parameters are found:

$$\begin{aligned} \theta = [&-0.137, 0.15, 0.0014, -0.0045, 0.00298, \\ &0.0000025, -0.000007, 0.000019, -0.000014] \end{aligned} \tag{6}$$

Using the estimated function $X_p(\alpha, \beta)$ (see (5) and (6)) in equations (3) and (4), and taking into account the *wipe-out property* (see [24]) to update the values of α and β in real-time, the Preisach model is simulated. Hysteresis curve for sinusoidal input of variable amplitude: 30, 60, 90 and 120 V and frequency of 1 Hz is presented in Fig. 5.

B. Hysteresis compensation with inverse multiplicative structure of Preisach model

The inverse of the Preisach model is generally constructed using numerical inversion [24], [25] since the input voltage signal $v_{px}(t)$ is implicitly involved in the complex dual integral formulation (1). To obtain the analytic inversion, one possible solution is the use of inverse multiplicative structure which has been initially developed for Bouc-Wen model [16] and subsequently extended to Preisach model [19].

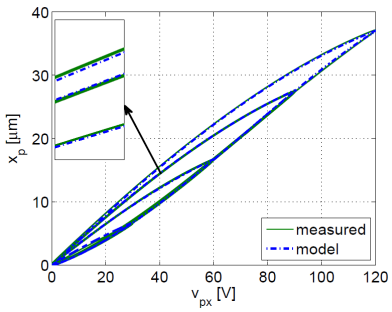

Fig. 5. Experimental and identified Preisach model of hysteresis for input signal of frequency 1 HZ and variable amplitude 30, 60, 90 and 120 V.

Assuming that exists a revertible function ρ such that the direct Preisach model $x_p(t) = H(v_{px}(t))$ (1) can be written as:

$$x_p(t) = \rho(v_{px}(t)) + \Gamma(v_{px}(t)) \tag{7}$$

For a desired expansion $x_p(t) = x_{p_r}(t)$, the required input voltage v_{px} can be expressed from (7) as:

$$v_{px}(t) = \rho^{-1}(v_{px}(t))[x_{p_r}(t) - \Gamma(v_{px}(t))] \tag{8}$$

where

$$\Gamma(v_{px}(t)) = H(v_{px}(t)) - \rho(v_{px}(t))v_{px}(t) \tag{9}$$

Taking into account the equations (7) and (8), the Preisach model and its exact inverse multiplicative structure that allows the design of the compensator analytically and without inversion of the model, are illustrated in Fig. 6. However, real-time

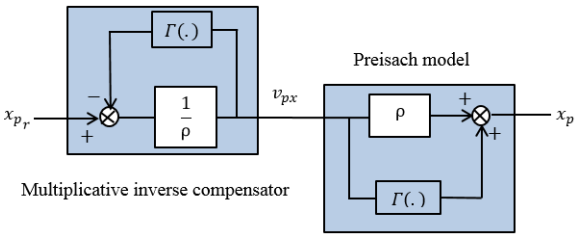

Fig. 6. The inverse multiplicative structure of the Preisach model.

implementation of (8) is compromised by the non-causality of the solution. To overcome this problem, the solution can be approximated as follows [17]:

$$v_{px}(t) = \rho^{-1}(v_{px}(t - T_s))[x_{p_r}(t) - \gamma(v_{px}(t - T_s))] \tag{10}$$

where T_s is the sampling time.
That leads to the so called approximate inverse multiplicative structure used in this work.

IV. Inverse Classical and Modified Prandtl-Ishlinskii Models

A. Classical and Modified Prandtl Ishlinskii Models

In this section so called classical Prandtl-Ishlinskii (PI) and Modified Prandtl-Ishlinskii (MPI) approaches are given [10], [13]. The elementary hysteresis operator of the classical PI

model is the backlash operator (see Fig. 7(a)), which plays the role of an elementary hysteretic mapping between the input signal $v_{px}(t)$ and the output displacement $x_p(t)$ of the piezoactuator as follows:

$$\begin{aligned} x_p(t) &= H_{x_{r_H}}[v_{px}, x_{p0}](t) \\ &= \max\{v_{px}(t) - r_{x_H}, \\ &\quad \min\{v_{px}(t) + r_{x_H}, x_p(t - T_s)\}\}, \end{aligned} \tag{11}$$

with r_{x_H} being an input threshold for v_{px} and T_s the sampling time. The classical PI model is a sum of weighted elementary backlash operators (Fig. 7(b)):

$$x_p(t) = H_x[v_{px}](t) = \boldsymbol{w}_{x_H}{}^T \boldsymbol{H}_{\boldsymbol{r}_{x_H}}[v_{px}, \boldsymbol{x}_{p0}](t), \tag{12}$$

where $\boldsymbol{r}_{x_H}$ is the vector of thresholds ($0 = r_{x_{H_0}} < r_{x_{H_1}} < ... < r_{x_{H_n}} < +\infty$), $\boldsymbol{w}_{x_H}$ is the vector of weights, $\boldsymbol{H}_{\boldsymbol{r}_{x_H}}$ is the vector of backlash operators and $\boldsymbol{x}_{p0}$ is the vector of initial states of the backlash operators.

The Modified Prandtl-Ishlinskii (MPI) model is composed of PI backlash operators followed by one-sided dead-zones. The output signal of a one-sided dead-zone operator (Fig. 7(c)) for an input signal $x_p(t)$ can be given by:

$$x_{p_s}(t) = S_{r_{x_S}}[x_p](t) = \begin{cases} \max\{x_p(t) - r_{x_S}, 0\}, & r_{x_S} > 0 \\ x_p(t), & r_{x_S} = 0 \end{cases} \tag{13}$$

where r_{x_S} is an input threshold for x_p.

The PI saturation operator S_x is the linear weighted superposition of dead-zone operators (see Fig. 7(d)):

$$x_{p_s}(t) = S_x[x_p](t) = \boldsymbol{w}_{x_S}{}^T \boldsymbol{S}_{\boldsymbol{r}_{x_S}}[x_p](t), \tag{14}$$

The MPI model is a cascade interconnection of the PI hysteresis model H_x defined by (12) and the PI saturation operator S_x defined by (14)

$$\begin{aligned} x_{p_s}(t) &= S_x[H_x[v_{px}]](t) \\ &= \boldsymbol{w}_{x_S}{}^T \boldsymbol{S}_{r_{x_S}}[\boldsymbol{w}_{x_H}{}^T \boldsymbol{H}_{r_{x_H}}[v_{px}, \boldsymbol{x}_{p0}]](t) \end{aligned} \tag{15}$$

where $\boldsymbol{r}_{x_S}$ is the vector of thresholds ($0 = r_{x_{S_0}} < r_{x_{S_1}} < ... < r_{x_{S_n}} < +\infty$) and $\boldsymbol{w}_{x_S}$ is the vector of weights.

The parameters to be identified are the weights of the backlashes $\boldsymbol{w}_{x_H}$ and the weights of the inverse dead-zones $\boldsymbol{w'}_{x_S}$. The identification procedure is as follows: (i) The threshold values $\boldsymbol{r}_{x_H}$ and $\boldsymbol{r}'_{x_S}$ and the initial states $\boldsymbol{x}_{p0}$ are set as follows:

$$r_{x_{H\,i}} = \frac{i}{n+1} max\{v_{px}\}, \quad i = 0, ..., n, \tag{16}$$

$$r'_{x_{S\,i}} = \frac{i}{m+1} max\{x_p\}, \quad i = 0, ..., m, \tag{17}$$

$$x_{p0_i} = 0, \quad i = 0, ..., n. \tag{18}$$

(ii) A triangular voltage input of variable amplitude: 30, 60, 90 and 120 V and of frequency 1 Hz is chosen as an identification signal. (iii) The Quadratic Programming algorithm of Matlab Optimization Toolbox™ is used to fit the model curve into the experimental data, by modification of weights

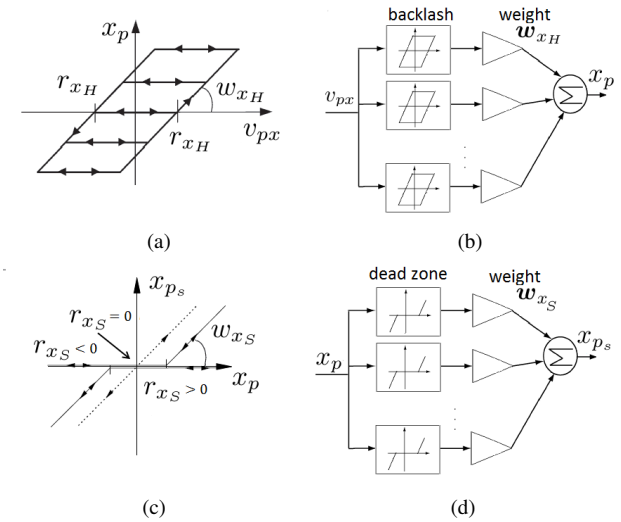

Fig. 7. (a) Weighted backlash operator. (b) Superposition of backlash operators. (c) Weighted dead-zone operator. (d) Superposition of dead-zone operators.

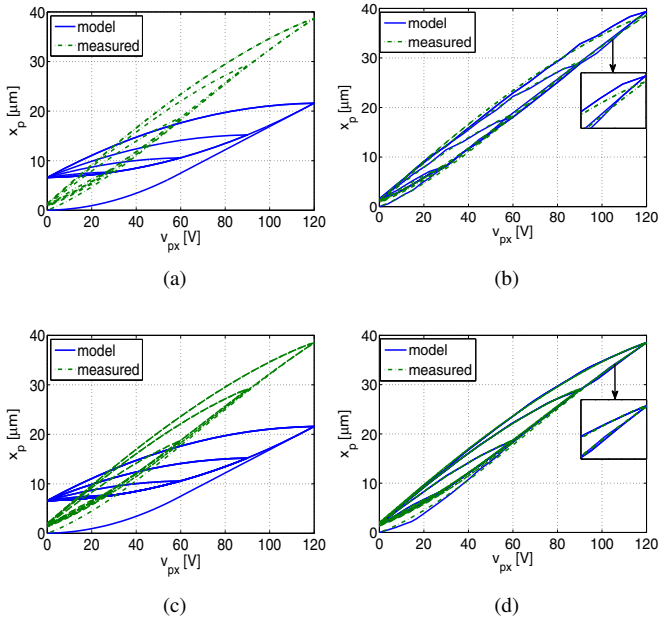

Fig. 8. Hysteresis identification: (a) Before identification (PI), (b) After identification (PI), (c) Before identification (MPI), (d) After identification (MPI).

$\boldsymbol{w}_x^T = \begin{bmatrix} \boldsymbol{w}_{x_H}^T & \boldsymbol{w}_{x_S}^{\prime T} \end{bmatrix}$ in order to minimize least-squares of the following error:

$$\begin{aligned} E_x[v_{px}, \tilde{x}_p](t) &= H_x[v_{px}](t) - S_x^{-1}[\tilde{x}_p](t) \\ &= \boldsymbol{w}_{x_H}^T \boldsymbol{H}_{r_{x_H}}[v_{px}, \boldsymbol{x}_{p0}](t) - \boldsymbol{w'}_{x_S}^T \boldsymbol{S}_{r'_{x_S}}[\tilde{x}_p](t) \end{aligned} \tag{19}$$

where $\tilde{x}_p(t) = \frac{y_1(t)}{G_{capx}}$ is a measured output displacement at time t. The model accuracy is determined by the number of backlashes $(n+1)$ and dead-zones $(m+1)$.

The thresholds $\boldsymbol{r}_{x_S}$ and the weights $\boldsymbol{w}_{x_S}$ of the dead-zones are calculated similarly as in equations (24) and (25),

respectively, using the thresholds $\boldsymbol{r}'_{x_S}$ and weights $\boldsymbol{w}'_{x_S}$ of the inverse dead-zones (for $i = 0, ..., m$).

Fig. 8(a) (resp. Fig. 8(c)) shows the experimental and the simulated hysteresis with the initial weights, while Fig. 8(b) (resp. Fig. 8(d)) presents the results after the identification procedure for PI (resp. MPI) approach.

Despite the chosen high accuracy ($n + 1 = 16$ backlashes), the PI model does not catches the saturation (see Fig. 8(b)), since it exhibits only symmetric hysteresis. This can be improved significantly using MPI approach (see Fig. 8(d)), where $n + 1 = 16$ backlashes and $m + 1 = 16$ dead-zone operators have been used.

The numerical values for the identified weights for PI (resp. MPI) model are given in equation (20) (resp. (21) and (22)).

$$\begin{aligned}\boldsymbol{w}_{x_H}^T =& 10^{-6} \cdot [0.1386, 0.1101, 0.0276, -0.0651, 0.1568,\\ & -0.0698, 0.0491, -0.0413, 0.0396, 0.0105,\\ & -0.0016, 0.0232, -0.0957, 0.0954, 0.0323,\\ & -0.0685]\end{aligned} \tag{20}$$

$$\begin{aligned}\boldsymbol{w}_{x_H}^T =& 10^{-6} \cdot [0.4001, 0.0492, 0.0814, -0.0242, 0.0886,\\ & 0.0074, 0.0548, 0.0265, -0.0374, 0.0378,\\ & 0.0093, 0.1146, -0.2047, 0.0989, 0.1547,\\ & -0.1286]\end{aligned} \tag{21}$$

$$\begin{aligned}\boldsymbol{w}_{x_S}^{'T} =& [3.0803, -1.2216, 0.1782, -0.2045, 0.0502,\\ & 0.0478, 0.0894, -0.0221, -0.0336, 0.0163,\\ & 0.0620, 0.2135, -0.0247, -0.1913, 0.4753,\\ & -0.2476]\end{aligned} \tag{22}$$

B. Hysteresis compensation with inverse Classical and Modified Prandtl-Ishlinskii models

To compensate for the hysteresis of the piezoactuator, its model is inverted and cascaded with the real system. For brevity, only the equations for inverse MPI model are given. The inverse of MPI model is expressed by:

$$\begin{aligned}v_{px}(t) &= H_x^{-1}[S_x^{-1}[x_{p_s}]](t)\\ &= \boldsymbol{w}'^{\,T}_{x_H} \boldsymbol{H}_{r'_{x_H}}[\boldsymbol{w}'^{\,T}_{x_S} \boldsymbol{S}_{r'_{x_S}}[x_{p_s}], \boldsymbol{v}_{px0}](t)\end{aligned} \tag{23}$$

with the transformed vector of thresholds $\boldsymbol{r}'_{x_H}$:

$$r'_{x_{H\,i}} = \sum_{j=0}^{i} w_{x_{H\,j}}(r_{x_{H\,i}} - r_{x_{H\,j}}), \quad i = 0, ..., n, \tag{24}$$

vector of weights $\boldsymbol{w}'_{x_H}$:

$$\begin{aligned}w'_{x_{H\,0}} &= \frac{1}{w_{x_{H\,0}}}, \quad i = 1, ..., n\\ w'_{x_{H\,i}} &= -\frac{w_{x_{H\,i}}}{\left(w_{x_{H\,0}} + \sum_{j=1}^{i} w_{x_{H\,j}}\right)\left(w_{x_{H\,0}} + \sum_{j=1}^{i-1} w_{x_{H\,j}}\right)},\end{aligned} \tag{25}$$

and vector of initial states $\boldsymbol{v}_{px0}$ of the inverted backlash operators:

$$v_{px0_i} = \sum_{j=0}^{i} w_{x_{H\,j}} x_{p0_i} + \sum_{j=i+1}^{n} w_{x_{H\,j}} x_{p0_j}, \quad i = 0, ..., n. \tag{26}$$

The inverse model of saturation operator has been already determined by $\boldsymbol{r}'_{x_S}$ (see (17)) and $\boldsymbol{w}'_{x_S}$ (found in the identification procedure (see (19)). The obtained MPI inverse model of hysteresis is cascaded with the plant as shown in Fig. 2.

V. Experimental results

In this section the experimental results for hysteresis compensation of piezoelectric actuator in the horizontal X axis of the 3DOF platform are given. Fig. 9 shows hysteresis compensation result for the considered methods. The difference between the approaches is highly observed in the saturation zone (see the inset in Fig. 9), for which the uncompensated system has 10 % of hysteresis. Due to its symmetrical property, the classical PI model lacks accuracy for high amplitudes for which the saturation occurs (the compensated system has 3.3 % of hysteresis). Unlike the PI model, the Preisach and MPI models can capture the asymmetric curves and the compensated system has 1.2 % and 0.5 % of hysteresis, respectively (the percentage of hysteresis in the saturation zone has been evaluated by taking the ratio between the hysteresis loop width and the displacement range). Tracking triangular waveform signals of frequency 1, 10 and 50 Hz are shown in Fig. 10(a), Fig. 10(c) and Fig. 10(e), respectively. The corresponding tracking errors are given in Fig. 10(b), Fig. 10(d) and Fig. 10(f)), respectively. The rms and maximal tracking errors for uncompensated and compensated system and for different scanning frequencies are given in Table I.

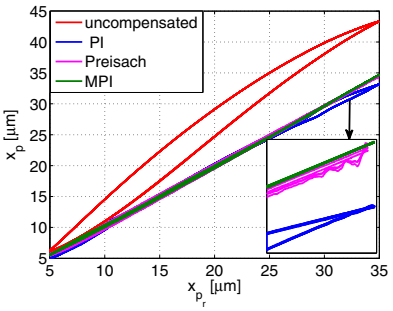

Fig. 9. Experimental hysteresis compensation for 1 Hz triangle input signal.

TABLE I
RMS AND MAXIMAL TRACKING ERROR - NUMERICAL VALUES

		uncomp	Preisach	PI	MPI
1 Hz	rms (μm)	4.6996	0.4182	0.7975	0.3133
	max (μm)	7.3042	0.8807	2.1765	0.6841
10 Hz	rms (μm)	4.6659	0.5522	0.9998	0.4436
	max (μm)	7.2417	1.3547	2.7494	0.9556
50 Hz	rms (μm)	4.660	1.1560	1.1797	0.9688
	max (μm)	7.4270	2.4660	3.0836	2.1547

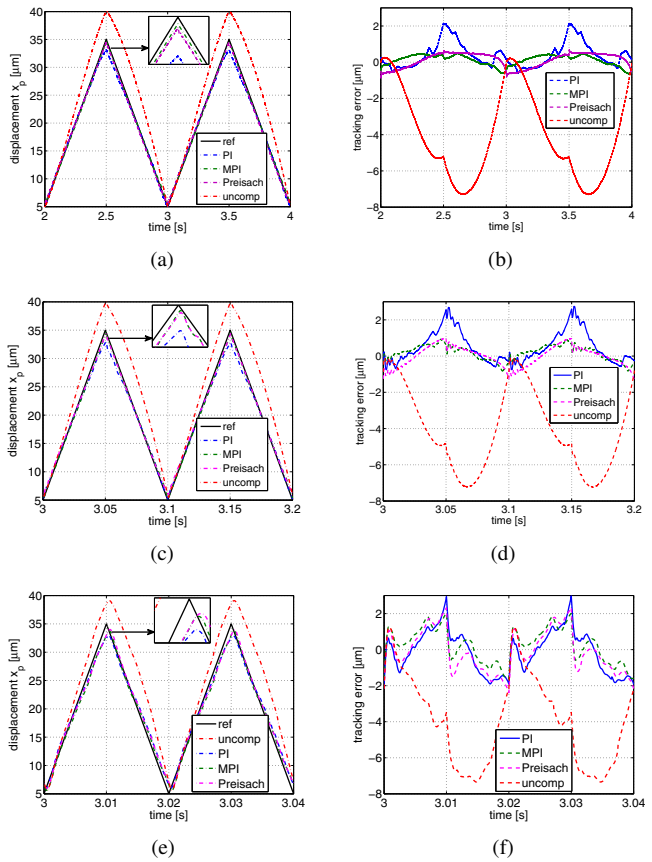

Fig. 10. Experimental results for triangular waveforms tracking: (a) 1HZ, (c) 10Hz, (e) 50Hz, corresponding tracking error: (b) 1HZ, (d) 10Hz, (f) 50Hz.

VI. Conclusion

In this paper inverse-based Preisach, PI and MPI approaches have been implemented and validated experimentally on the horizontal (X) axis of a 3DOF micro-/nanopositioning platform. The obtained results show that in all cases a significant improvement can be achieved w.r.t. any compensation. Though still computationally intensive, the multiplicative inverse structure of the Preisach model allows to avoid model inversion numerically and gives good results for asymmetric hysteresis. The classical PI model is analytic and less time-consuming. However, it gives satisfactory results only for reasonably small input voltages and its performance deteriorates for higher amplitudes due to its property of symmetry. The experimental results confirm, that the MPI model has all the advantages of its classical counterpart and generalizes it for asymmetric hysteresis loops, thus making it both accurate and suitable for real-time implementation.

References

[1] G. Binning and H. Rohrer, "Scanning Tunneling Microscopy", *IBM Journal of Research and Development*, vol. 30, no. 4, pp. 355-369, 1986.

[2] G. Binning, C. F. Quate, and Ch. Gerber, "Atomic Force Microscope", *Physical Review Letters*, vol. 56, no .9, pp. 930-933, 1986.

[3] D. Y. Abramovitch, S. B. Andersson, L. Y. Pao, and G. Schitter, "A Tutorial on the Mechanisms, Dynamics, and Control of Atomic Force Microscopes", *ACC 2007*, pp. 3488-3502, Jul. 2007.

[4] K. K. Leang and S. Devasia, "Feedback-linearized inverse feedforward for creep, hysteresis, and vibration compensation in AFM piezoactuators", *IEEE Trans. on Control Systems Technology*, vol. 15, no. 5, pp. 927-935, 2007.

[5] M. S. Tsai and J. S. Chen, "Robust tracking control of a piezoactuator using a new approximate hysteresis model", *Journal of dynamic systems, measurement, and control*, vol. 125, no. 1, pp. 96-102, 2003.

[6] J. Yi, S. Chang and Y. Shen, "Disturbance-observer-based hysteresis compensation for piezoelectric actuators", *IEEE/ASME Trans. on Mechatronics*, vol. 14, no. 4, pp. 456-464, 2009.

[7] Ł. Ryba, A. Voda, and G. Besançon, "An LQG/LTR approach towards piezoactuator vibration reduction with observer-based hysteresis compensation", *The 19th IFAC World Congress*, pp. 5623-5628, Aug. 2014.

[8] J. Schäfer, H. Jürgen, "Compensation of hysteresis in solid-state actuators", *Sensors and Actuators A: Physical*, vol. 49, no. 1, pp. 97-102, 1995.

[9] S. Xiao, Shunli and Li, Yangmin, "Modeling and high dynamic compensating the rate-dependent hysteresis of piezoelectric actuators via a novel modified inverse Preisach model", *IEEE Trans. on Control Systems Technology*, vol. 21, no. 5, pp. 1549-1557, 2013.

[10] K. Kuhnen and H. Janocha, "Inverse feedforward controller for complex hysteretic nonlinearities in smart-material systems", *Control and Intelligent systems*, vol. 29, no. 3, pp. 74-83, 2001.

[11] M. Rakotondrabe, C. Clévy, and P. Lutz, "Complete Open Loop Control of Hysteretic, Creeped and Oscillating Piezoelectric Cantilevers", *IEEE Trans. on Autom. Science and Eng.*, vol. 7, no. 3, pp. 440-450, Jul. 2010.

[12] Ł. Ryba, A. Voda, and G. Besançon, "Modelling and control of 3D STM-like scanning device with application to surface reconstruction", *Proc of 18th Int. Conf. on MMAR*, pp. 479-484, Aug. 2013.

[13] K. Kuhnen, "Modeling, identification and compensation of complex hysteretic nonlinearities: A Modified Prandtl-Ishlinskii approach", *European Journal of Control*, vol. 9, no. 4, pp. 407-418, 2001.

[14] T. Butz and O. Von Stryk "Modelling and simulation of electro-and magnetorheological fluid dampers", *Journal of applied mathematics and mechanics (ZAMM)*, vol. 82, no. 1, pp. 3-20, 2002.

[15] D. Croft, G. Shed, and S. Devasia, "Creep, hysteresis, and vibration compensation for piezoactuators: Atomic force microscopy application", *ACC 2000*, vol. 3, pp. 2123-2128, 2000.

[16] M. Rakotondrabe, "Bouc-Wen Modeling and Inverse Multiplicative Structure to Compensate Hysteresis Nonlinearity in Piezoelectric Actuators", *IEEE Trans. on Automation Science and Engineering*, vol. 8, no. 2, pp. 428-431, Apr. 2011.

[17] M. Rakotondrabe, "Classical Prandtl-Ishlinskii modeling and inverse multiplicative structure to compensate hysteresis in piezoactuators", *ACC 2012*, pp. 1646-1651, June 2012.

[18] I. D. Mayergoyz, *Mathematical models of hysteresis and their applications*, 2003.

[19] Z. Li, C. Y. Su, T. Chai, "Compensate of hysteresis nonlinearity in magnetostrictive actuators with inverse multiplicative structure for Preisach model", *IEEE Trans. on Automation Science and Engineering*, vol. 11, no. 2, pp. 613-619, Apr. 2014.

[20] H. Janocha and K. Kuhnen, "Real-time compensation of hysteresis and creep in piezoelectric actuators", *Sensors and actuators A: Physical*, vol. 79, no. 2, pp. 83-89, 2000.

[21] G. Y. Gu, L. M. Zhu, and Ch. Y. Su, "Modeling and Compensation of Asymmetric Hysteresis Nonlinearity for Piezoceramic Actuators With a Modified Prandtl-Ishlinskii Model", *IEEE Trans. On Industral Electronics*, vol. 61, no. 3, pp. 1583-1595, Mar. 2014.

[22] S. Bobbio and G. Marrucci, "A possible alternative to Preisach's model of static hysteresis", *Il Nuovo Cimento D*, vol. 15, no. 5, pp. 723-733, 1993.

[23] Ł. Ryba, A. Voda, and G. Besançon, "3DOF nanopositioning control of an experimental tunneling current-based platform", *IEEE Multiconference on Systems and Control (MSC 20014)*, pp. 1976-1981, Oct. 2014.

[24] X. Zhou, J.Zhao, G. Song and J. De Abreu-Garcia, "Preisach Modeling of Hysteresis and Tracking Control of a Thunder Actuator System", *Smart Structures and Materials*, pp. 112-125, Mar. 2003.

[25] G. Song, J. Zhao, X. Zhou and J.A. De Abreu-Garcia, "Tracking control of a piezoceramic actuator with hysteresis compensation using inverse Preisach model", *IEEE/ASME Trans. on Mechatronics*, vol. 10, no. 2, pp. 198-209, Apr. 2005.